

Boundary effects in large-aspect-ratio lasers

G. K. Harkness and W. J. Firth

Department of Physics and Applied Physics, University of Strathclyde, Glasgow G4 0NG, Scotland

J. B. Geddes and J. V. Moloney

Department of Mathematics, University of Arizona, Tucson Arizona 85721

E. M. Wright

Optical Sciences Center, University of Arizona, Tucson, Arizona 85721

(Received 16 May 1994)

We study theoretically the effect of transverse boundary conditions on the traveling waves found in infinitely extended and positively detuned laser systems. We find that for large-aspect-ratio systems, well above threshold and away from the boundaries, the traveling waves persist. Source and sink defects are observed on the boundaries, and in very-large-aspect-ratio systems these defects can also exist away from the boundaries. The transverse size of the sink defect, relative to the size of the transverse domain, is important in determining the final pattern observed, and so, close to threshold, standing waves are always observed.

PACS number(s): 42.50.Ne, 42.55.-f, 47.20.Ky

I. INTRODUCTION

Pattern formation in the transverse plane of a laser beam is an interesting and challenging area of research in nonlinear optics. Models taking into account the transverse structure of the electric field and laser medium variables fall into two main categories, the main distinction has been that of *aspect ratio*. Real lasers have some form of confinement in the transverse plane which could be provided by intracavity apertures, curved cavity mirrors, or using a spatially dependent pump. One definition of aspect ratio is the ratio of this transverse confinement length to the fundamental scale of the laser pattern. The work of Lugiato *et al.* [1] and subsequent work by others [2] concentrates on small-aspect-ratio systems in which the beam is strongly confined on the transverse length scale of the pattern. In their case the transverse confinement is induced by curved cavity mirrors and the dynamics is composed of a relatively small number of transverse cavity modes—Gauss-Laguerre modes. Large-aspect-ratio systems, usually with plane cavity mirrors and of infinite transverse extent, have been considered by Coulet *et al.* [3,4] and others. In such a system, Jakobsen *et al.* [5] showed that the Maxwell-Bloch equations describing a two-level ring laser have exact transverse traveling-wave solutions. These correspond to off-axis emissions from the laser and are selected to allow it to lase with the lowest possible threshold, that is, at line center. This threshold behavior was previously noted by Gil in 1988 [6].

Both approaches have shown that laser systems can exhibit complex spatiotemporal behavior including optical vortices and optical turbulence. These observations, along with work [3,7] which showed that laser models could be reduced to a complex form of the Ginzburg-Landau equation used in fluid dynamics, led to analogies

being drawn between the pattern formation in the fields of optics and hydrodynamics.

In this paper we will study the traveling-wave (TW) solutions in a large-aspect-ratio laser system following the approach developed in hydrodynamics for the study of their pattern forming properties, defects, and instabilities [8,9].

The effects of transverse boundary conditions on models with an underlying traveling wave can be very important. Based on a set of amplitude equations, valid close to the threshold for pattern formation, Cross [10] analyzed the effects of finite geometries on the traveling waves found in hydrodynamic systems. His work was, however, limited to one transverse dimension. In this paper, we analyze the full complex Lorenz system, describing a laser, to determine the effects of “zero” boundary conditions on the laser field at the edge of finite transverse domains, in both one and two dimensions.

In Sec. II we introduce the model set of equations for the problem of the single longitudinal mode laser with infinitely extended plane, parallel mirrors [9]. In Sec. III we review the results on the analysis of these equations. In Sec. IV we present our results on the model with zero boundary conditions in the transverse plane.

II. TWO-LEVEL LASER MODEL

The complex Lorenz form of the Maxwell-Bloch equations

$$\begin{aligned} \frac{\partial e}{\partial t} &= ia\nabla_T^2 e - \sigma e + \sigma p, \\ \frac{\partial p}{\partial t} &= re - (1 + i\Delta)p - ne, \\ \frac{\partial n}{\partial t} &= -bn + \frac{1}{2}(ep^* + e^*p), \end{aligned} \quad (1)$$

describes the behavior of the complex electric field e , the complex polarization p , and the real population inversion n in a two-level ring laser with a single longitudinal cavity mode and plane cavity mirrors [9]. A mean field approach has been used to remove the dependence of the longitudinal coordinate and so these variables depend only on the transverse coordinates and time [1]. The parameter a is the diffraction parameter, σ is the decay rate of the field due to cavity losses, b is the population decay rate, and Δ is the detuning between the longitudinal cavity mode frequency and atomic resonance $\Delta = (\omega_a - \omega_c)/\gamma_\perp$. All decay rates, frequencies, and time are scaled to the decay rate of the polarization γ_\perp . The strength of the pumping is characterized by the “stress parameter” r . Note that we have omitted the effects of carrier diffusion in the equation for n [5]; this is for reasons of simplicity. We do not expect carrier diffusion to greatly affect the physical relevance of the results presented here.

III. REVIEW OF TW ANALYSIS

A. Traveling waves

Jakobsen *et al.* [5] have shown that the lasing solutions to the complex Lorenz equations (1) have different character depending on the sign of the detuning Δ . For $\Delta < 0$, the bifurcation at the first laser threshold is to a uniform plane wave state and will not be further discussed herein. We will concentrate on the case of $\Delta > 0$, where the equations have *exact* traveling-wave solutions with transverse wave vector \mathbf{k}_0 ,

$$\begin{pmatrix} e \\ p \\ n \end{pmatrix} = \begin{pmatrix} e_0 \\ p_0 \\ n_0 \end{pmatrix} = \begin{pmatrix} A \exp(i\mathbf{k}_0 \cdot \mathbf{r} - i\Omega t) \\ A\chi \exp(i\mathbf{k}_0 \cdot \mathbf{r} - i\Omega t) \\ r - |\chi|^2 \end{pmatrix}, \quad (2)$$

where

$$\begin{aligned} \chi &= 1 - i(\Delta - \Omega), \\ \Omega &= \frac{\sigma\Delta + a|\mathbf{k}_0|^2}{\sigma + 1}, \\ |A|^2 &= bn_0. \end{aligned} \quad (3)$$

This traveling wave corresponds to an off-axis emission from the laser. The threshold $r_{\text{th}}(k_0)$ for any such traveling wave is obtained by setting $|A|^2 = 0$, which implies $n_0 = 0$, in Eqs. (2) and (3)

$$r_{\text{th}}(k_0) = 1 + \left(\frac{\Delta - a|\mathbf{k}_0|^2}{\sigma + 1} \right)^2.$$

The curve $r_{\text{th}}(k_0)$ is called the *neutral stability curve* and is plotted in Fig. 1. The minimum of this curve, that is the traveling wave with the lowest threshold, is for $|\mathbf{k}_0| = k_c = \sqrt{\Delta/a}$ and so we expect the traveling wave with this wave vector to be the one selected at the first laser threshold $r_{\text{th}}(k_c) = 1$. For this case, $\Omega = \Delta$, i.e., the laser operates on resonance. Physically, the longitudinal wave vector of the laser field is “tilted” by k_c so as to make it resonant with the atomic transition.

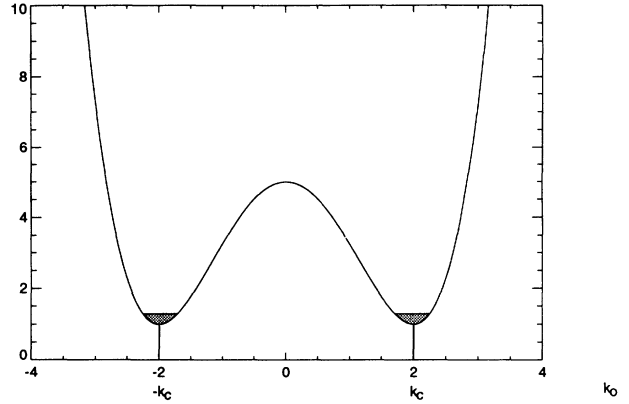


FIG. 1. Neutral stability curve for traveling waves at the first laser threshold. Parameters are $a = 1$, $b = 1$, $\Delta = 4$, and $\sigma = 1$.

Figure 1 shows that for $r > 1$ a band of wave vectors around k_c can be excited. Since the neutral stability curve depends only on modulus of the transverse wave vector $|\mathbf{k}_0|$, not its direction, a whole annulus of wave vectors can become active. It is a remarkable feature of this system that a two-dimensional continuum of *exact* solutions exists above the neutral stability curve. These solutions assume the presence of only a single wave vector, however, and so can be exhibited only if a single wave vector \mathbf{k}_0 is able to dominate and suppress all others. The process by which that occurs, and the ways in which it can be inhibited by boundaries, is the main topic of this paper. The *stability* of the TW solutions is also important and is summarized in Sec. III D.

B. Amplitude equations

The nonlinear competition between the active modes can be captured analytically through the derivation of *universal amplitude equations* for the system. The equations are universal insofar as their form is determined solely by the nonlinearities and symmetry properties of the system [8,11]; all the specific details of the system are contained in the coefficients [5,9]. For the one-dimensional case, the complex amplitudes involved, F and B , are those of the forward and backward traveling waves with wave vector k_c . The amplitude equations below are only valid close to threshold since their derivation involves an expansion of the amplitude and the space and time scales in terms of a smallness parameter $\varepsilon = (r - 1)^{1/2}$,

$$\begin{aligned} (\sigma + 1) \frac{\partial F}{\partial t} + 2ak_c \frac{\partial F}{\partial x} \\ = ia\nabla^2 F - \frac{\sigma a^2}{(\sigma + 1)^2} \left(2ik_c \frac{\partial}{\partial x} + \frac{\partial^2}{\partial y^2} \right)^2 F \\ + \sigma(r - 1)F - \frac{\sigma}{b} (|F|^2 + 2|B|^2) F, \end{aligned} \quad (4a)$$

$$\begin{aligned}
& (\sigma + 1) \frac{\partial B}{\partial t} - 2ak_c \frac{\partial B}{\partial x} \\
& = ia\nabla^2 B - \frac{\sigma a^2}{(\sigma + 1)^2} \left(2ik_c \frac{\partial}{\partial x} + \frac{\partial^2}{\partial y^2} \right)^2 B \\
& + \sigma(r - 1)B - \frac{\sigma}{b} (|B|^2 + 2|F|^2) B. \quad (4b)
\end{aligned}$$

These equations are in the form of coupled complex Newell-Whitehead-Segel equations. In one transverse dimension [5] ($\partial/\partial y \rightarrow 0$) these equations reduce to coupled complex Ginzburg-Landau (CGL) equations. Table I shows the steady state solutions of the CGL equations, independent of the transverse coordinates. The results of a linear stability analysis of these solutions are shown in Fig. 2. Above threshold, the only stable solution is the traveling wave and so, at least with one transverse dimension, one of the traveling-wave solutions suppresses the other. Thus we have a winner-takes-all competition between two stable solutions. When we consider two transverse dimensions we expect the ring of active modes to collapse to a single point in k space and this is indeed what happens.

If carrier diffusion were to be included in the original Lorenz model, then the effect on the amplitude equations (4) would be to reduce the coefficient of the nonlinear cross coupling terms [5]. This coefficient will always be greater than 1 and so the results of the above stability analysis are still valid no matter how strong the carrier diffusion.

C. Numerical simulations: Qualitative results

Numerical simulations of the complex Lorenz equations, using periodic transverse boundary conditions to simulate the infinite transverse extent of the system, have been performed [5] and confirm that, above threshold, a single traveling-wave solution is indeed selected. Periodic boundary conditions are not exactly equivalent to infinite transverse extent and it is interesting to compare the results of simulations with different sizes L of computational domains. Our numerical simulations for relatively small, one-dimensional, transverse domains¹ $L \approx 8 \times 2\pi/k_c$ and initial conditions of some noise around zero show that the entire domain switches on to a single

TABLE I. Steady states of the coupled CGL equations without spatial derivatives

$ F ^2$	$ B ^2$	State
0	0	nonlasing
$b(r - 1)/3$	$b(r - 1)/3$	lasing, standing wave
$b(r - 1)$	0	lasing, forward traveling wave
0	$b(r - 1)$	lasing, backward traveling wave

¹Note that the corresponding physical sizes of the domains depend greatly on the parameters chosen for the system.

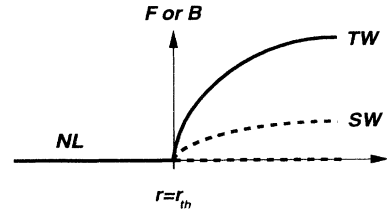


FIG. 2. Bifurcation diagram showing the solutions of the space-independent amplitude equations (4) and their stability as a function of the pump parameter r . TW, traveling wave; SW, standing wave; NL, nonlasing. Solid lines are stable solutions and dashed lines are unstable.

traveling wave. Whether it is the forward or backward traveling wave which is selected is determined solely by the noise in the system. For domains of twice this size, or larger, it is possible for there to exist regions of the transverse domain which have traveling waves propagating in different directions, as shown diagrammatically in Fig. 3. These regions of different traveling waves are connected by *defects* of the system. Coulet *et al.* [12] have termed these defects *source* and *sink* reflecting their character as either a source of traveling waves or as a sink. At the core of the sink defect the amplitudes F and B are both large, whereas at the core of the source defect both amplitudes are small. Regions where the amplitudes of both the forward and backward traveling waves are comparable correspond to localized transverse standing waves of the electric field in the laser. Therefore, the sink defect appears as a localized standing wave and the source defect does not. In the dynamics of the pattern, the defects undergo a relatively slow motion. Such defects will be very important later in this paper for our understanding of the patterns obtained with the reflecting transverse boundary conditions.

D. Stability of traveling waves

We have shown that the complex Lorenz equations show traveling-wave solutions and that these are the preferred solutions just above threshold. What of their stability above threshold? The stability analysis of the traveling waves has been approached in a number of ways. Since there exists an exact traveling-wave solution, its linear stability can be tested in the usual way. This is the most powerful technique as it omits no classes of instability. The problem is that, since it involves finding the eigenvalues of a complex 5×5 matrix, it is inevitably

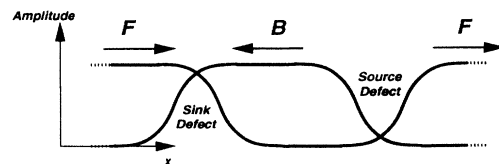


FIG. 3. Diagrammatic representation of the source and sink defects.

numerical in practice and offers little physical insight into the problem. Another technique, based on the amplitude equations (4), gives more insight, but is only valid close to threshold and, because the amplitudes may vary only slowly in space, it only tests for instability to nearby wave vectors, i.e., it is a long wavelength limit of the full linear stability analysis. A further technique, based on the derivation of a Cross-Newell phase equation for the system, has been used by Lega *et al.* [13]. This removes the constraint of being close to threshold, but still tests only for instability to nearby wavevectors.

Figure 4 shows the result of these stability analyses. An area on this diagram where traveling waves are stable is known as a *Busse balloon* [14]. The lowest curve is the neutral stability curve for the existence of traveling waves. The light grey area is the Busse balloon computed from the phase equation method and the darker grey area is the Busse balloon computed numerically from the full stability analysis. Close to threshold the balloons coincide, but further above threshold and for k_0 far from k_c they differ. One major difference is that the darker grey area starts to close again for increasing r . This is due to the presence of an *amplitude instability* [5,15]—when the traveling waves become unstable to sidebands at $k_0 \pm k_s$. This stability diagram has been verified by direct numerical simulations of the Lorenz system. For the parameter values we will consider in the rest of this paper—specifically the stress parameter r —the amplitude instability is not a factor. Note that Fig. 4 may be rotated about the vertical axis and that the Busse balloon thus contains, at each value of r , a twofold continuum of stable traveling waves.

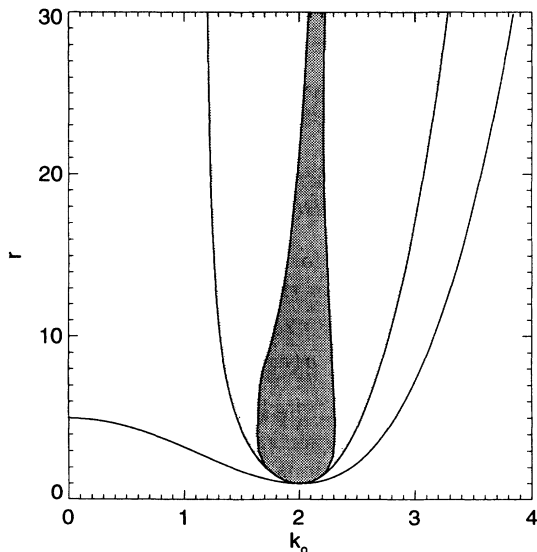


FIG. 4. Results of the stability analysis for traveling waves. Grey areas represent the Busse balloons calculated analytically from the Cross-Newell phase equation (light grey) and computed from the full stability analysis (dark grey). System parameters are $a = 1$, $b = 1$, $\Delta = 4$, and $\sigma = 1$.

IV. REFLECTING BOUNDARIES

We now study the effects of transverse boundaries on the traveling waves seen in the infinitely extended system. We consider the case of a dielectric waveguide in the appropriate limit so that the electric field inside obeys the condition $e(x, y) = 0$ on the boundary [16]; $p(x, y)$ and $n(x, y)$ obey the same condition. We performed numerical simulations of the Lorenz equations with these boundary conditions with both one and two transverse dimensions. The method used was of the split-step Fourier type with the diffraction step being solved spectrally, using a “fast sine transform,” and the nonlinear step using a second-order Runge-Kutta method [17].

A. One transverse dimension

First, for simplicity, we considered only one transverse dimension. A typical asymptotic state of the system is shown in Fig. 5. The results show that a localized standing wave appears at one of the boundaries. At the other boundary the field goes to zero without a standing wave.

Although with the reflecting boundary conditions in force the traveling-wave solutions are no longer exact, we expect them to be a good basis in which to describe the patterns. Indeed, we can understand this pattern in terms of the amplitudes of the forward and backward traveling waves of the infinitely extended system.

Consider the electric field to be a sum of forward and backward traveling waves with amplitudes $F(x)$ and $B(x)$. The boundary conditions are $e(0) = e(L) = 0$, which are, in terms of the traveling-wave amplitudes,

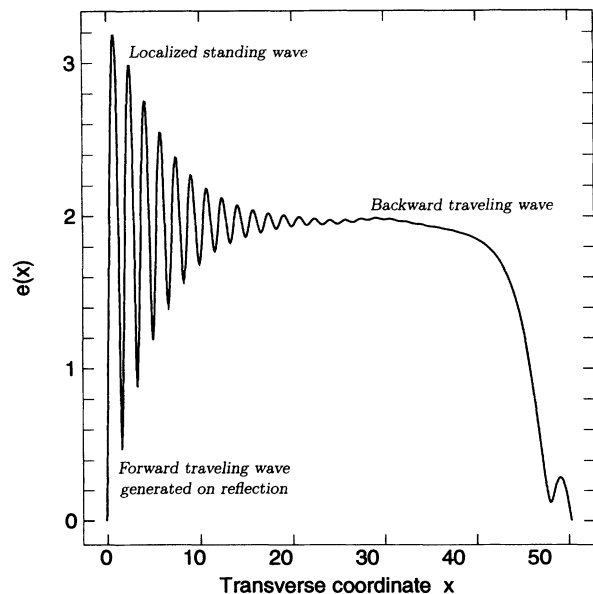


FIG. 5. Modulus of the electric field $|e|$ as a function of transverse space coordinate x for a domain width $L \approx 50$ $a = 1$, $b = 1$, $\Delta = 4$, $\sigma = 1$, and $r = 5$.

$F(x) = -B(x)$ for $x = 0, L$. At the center of a sufficiently wide transverse domain we expect the system to behave in a similar way to the infinitely extended system, namely, that one of the traveling waves will dominate; see Fig. 6. Which one dominates depends on chance through the initial conditions. In Fig. 5 the backward traveling wave dominates in the center. As the wave travels backwards it reaches the left-hand boundary and reflects, generating a forward traveling wave. So, close to this boundary we see an area with both forward and backward traveling waves, which looks like a standing wave in the electric field. It has already been shown that, at least for the infinitely extended system, this standing wave solution is unstable. The forward traveling wave is therefore suppressed and the standing wave is thus localized.

Close to the right-hand boundary and in the initial "switch-on" phase of the laser both forward and backward waves will be generated and the winner will be determined by their nonlinear competition. The backward wave is reinforced by the reflection of the forward wave and so dominates, propagating back to the center.

These localized structures seen near the boundaries are, in fact, the defects of the infinitely extended system mentioned in Sec. III C. If we imagine the system reflected in the left-hand boundary, then that boundary is being fed by traveling waves from both sides—it is the sink defect. At the right-hand boundary, the traveling waves are propagating away and so this is the source defect. Figure 5 shows that the defects are quite well localized at the boundaries. If the boundaries were to be brought closer together, i.e., the laser's aspect ratio was reduced, or if the parameters were changed to increase the transverse size of the defects, then it may no longer be useful to use the traveling-wave description for the laser.

The transverse size of the defects relative to the size of the transverse domain is obviously very important in determining the pattern which will be selected by the laser. In fact, the source and sink defects behave very differently in this system. The sink defect's size diverges to infinity as the laser is brought close to threshold (that is,

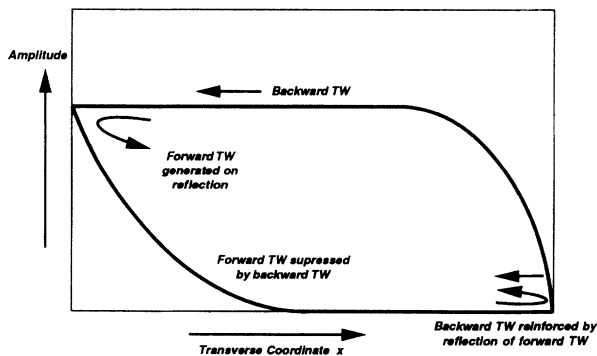


FIG. 6. Diagrammatic representation of the amplitudes of the forward and backward traveling-wave amplitudes as a function of the transverse coordinate x and how these amplitudes combine to make the pattern in Fig. 5.

$r \rightarrow 1$), while the source defect shows more complicated behavior. Coulet *et al.* [12] studied these defects in the CGL equation and they have shown that because of the finite velocity of the traveling waves in the system, the size of the source defect diverges to infinity at some critical value of the pump $r_c \gg 1$. This would, theoretically, lead to the whole transverse domain switching to the zero state, but this will not happen in practice because any small amount of noise, either in a real experiment or due to numerical inaccuracies, will seed the traveling-wave solution again. What is seen, in the laser case, is that the source defect develops a series of "blips" which propagate away from the source towards a sink. One such blip can be seen in Fig. 5 close to the right-hand boundary. So, as the laser is brought close to threshold, the size of the source defect increases and saturates to a value determined by the noise in the system while the size of the sink defect increases unchecked. Consequently, it is the size of the sink defect compared to the size of the transverse domain that is important here.

Figure 7 shows the results of two numerical simulations for which the size of the sink defect becomes comparable to the size of the transverse domain. In Fig. 7(a) the size of the domain is made smaller than the defect size and in Fig. 7(b) the size of the sink defect is made large by reducing the pump parameter r closer to threshold.

We have attempted to obtain an analytical measure for the size of the sink defect using a method based on the amplitude equations. As Figs. 5 and 6 show, at the sink defect the decay of the forward traveling-wave amplitude is almost exponential and the amplitude of the backward traveling wave is almost constant and equal to the amplitude predicted by the amplitude equations (4). This has been verified more quantitatively. We look for time-independent solutions of the amplitude equations without diffraction,

$$\begin{aligned} 2ak_c \frac{\partial F}{\partial x} &= \sigma(r-1)F - \frac{\sigma}{b} (|F|^2 + 2|B|^2) F, \\ -2ak_c \frac{\partial B}{\partial x} &= \sigma(r-1)B - \frac{\sigma}{b} (|B|^2 + 2|F|^2) B, \end{aligned}$$

and substitute

$$F(x) = F_0 e^{-x/l}, B(x) = [b(r-1)]^{1/2}. \quad (5)$$

The linearized equation for F around $F = 0$ now gives an estimate for the size of the sink defect,

$$l \approx \frac{2ak_c}{\sigma(r-1)}.$$

Figure 8 shows a graph of the sink defect size l as a function of the pump parameter r . For comparison, we performed numerical simulations of the complex Lorenz system, extracted the amplitudes of the forward and backward traveling waves, using a localized Fourier integral method, and found the value of l in (5) which gave the best fit to the data. These data points are also shown in Fig. 8. The estimates calculated from the amplitude equations do not agree too well quantitatively with the numerics, but the qualitative behavior is correct. That l is underestimated is not surprising in view of the fact

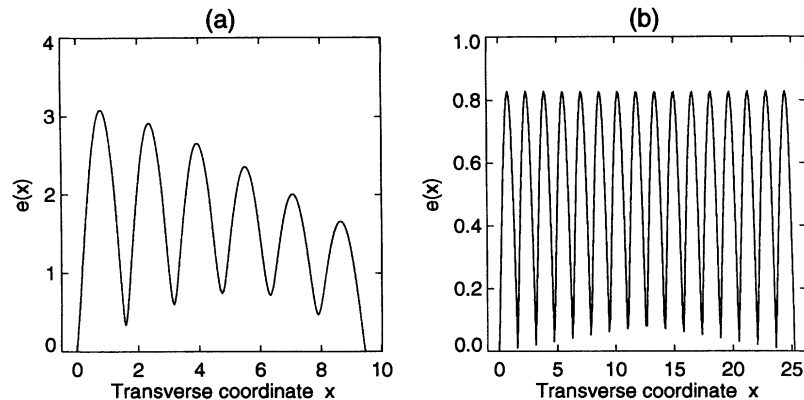


FIG. 7. Modulus of the electric field $|e|$ as a function of transverse space coordinate x . Parameters are $a = 1$, $b = 1$, $\Delta = 4$, and $\sigma = 1$: (a) has domain width $L \approx 9.5$ and $r = 5$ and (b) has domain width $L \approx 25$ and $r = 1.5$.

that the above assumes a constant suppression factor for F by B , whereas the factor must actually go to zero at the core of the defect.

Figure 9 shows the results of a simulation with a domain width $L = 100$, double that of Fig. 5. The sink defect is now in the center of the domain, being fed by traveling waves from source defects on each boundary. Note that the size of the sink defect is the same as that in Fig. 5, showing that the size of the defects are insensitive to the size of the transverse domain. For still wider transverse domains complex arrays of source and sink defects form and annihilate (see Fig. 10) as part of the dynamics.

B. Two transverse dimensions

We now consider the problem of reflecting boundaries on a two-dimensional transverse domain. We will first

consider a square domain characterized by the Cartesian coordinates (x, y) . The analysis of the one-dimensional problem in Sec. IV A leads us to expect to see localized standing waves close to one of the boundaries. Figure 11 is a frame from a movie showing the result of a numerical simulation of the complex Lorenz equations (1) with zero boundary conditions on a square. The size of the transverse domain is approximately 50×50 units and so this figure is basically the two transverse dimension analog of Fig. 5. It appears that the sink defect is positioned along the upper and right edges of the square; the source defect is located near the bottom left-hand corner. The blips seen in the one-dimensional simulations (Fig. 5) manifest themselves as optical vortices in two dimensions. These vortices are born at the source and are swept across the domain in the direction of the traveling wave towards the sink. The generation of these vortices is attributed to the instability of the source defect described in Sec. IV A. We performed numerical simulations with parameter values

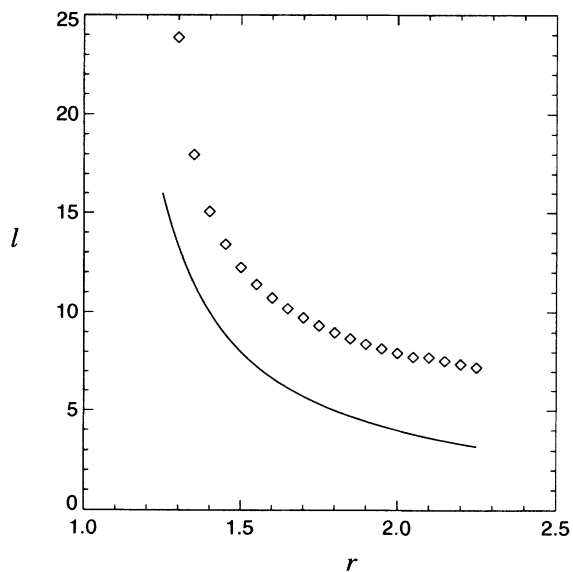


FIG. 8. Characteristic size l of the sink defect extracted from the numerical simulations (diamonds) and computed from the amplitude equations (full line) plotted versus the pump parameter r . Other parameters are $a = 1$, $b = 1$, $\Delta = 4$, and $\sigma = 1$.

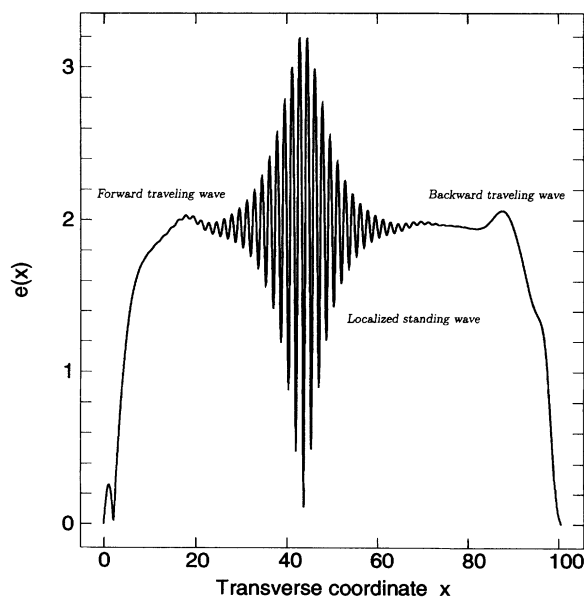


FIG. 9. Modulus of the electric field $|e|$ as a function of transverse space coordinate x for a domain width $L \approx 100$. $a = 1$, $b = 1$, $\Delta = 4$, and $\sigma = 1$, and $r = 5$.

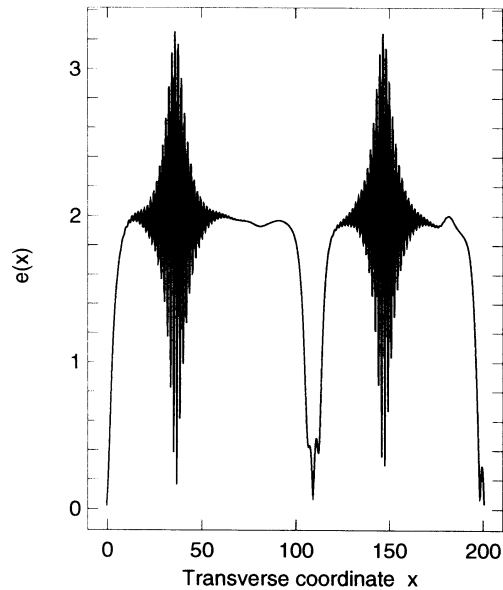


FIG. 10. Modulus of the electric field $|e|$ as a function of transverse space coordinate x for a domain width $L = 200$. $a = 1$, $b = 1$, $\Delta = 4$, $\sigma = 1$, and $r = 5$.

for which the source defect is stable and we observe a stationary pattern without vortices. Note that there is a huge difference between the zeros of the field associated with these vortex defects in the bottom left of Fig. 11 and the phase singularities at the nodes of the standing wave at the top right. The size of the vortex defects

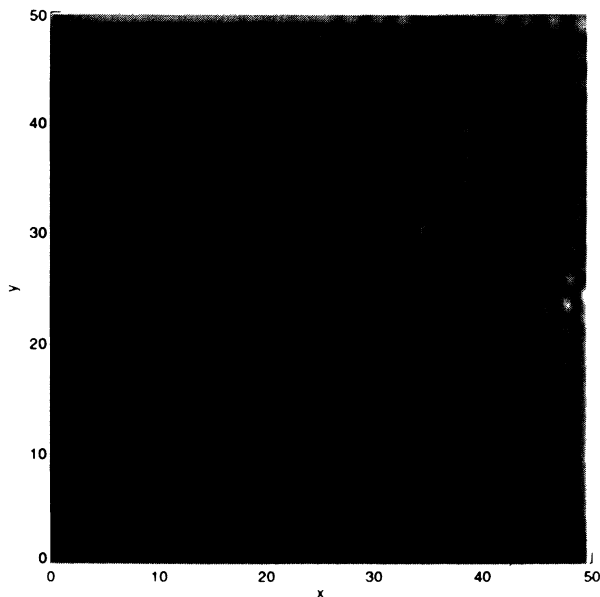


FIG. 11. Modulus of the electric field $|e|$ as a function of the two transverse coordinates (x, y) for a domain width $L \approx 50$. $a = 1$, $b = 1$, $\Delta = 4$, $\sigma = 1$, and $r = 5$. White means high intensity and black means low intensity. The three dark patches at the lower left are vortex defects, which convect with the traveling wave to the sink at the upper right.

depends on the spatial growth rate away from the zero of the field, which depends on the value of the pump. The size of the standing-wave nodes, however, is determined solely by the wavevector of the dominant TW and is therefore pump independent.

We should point out that both the sink and the source are line defects. We have checked this by performing simulations with the upper and lower domain walls being reflecting and the left and right walls periodic. The simulations show that the sources and sinks line up along the reflecting boundaries and are stable in that position. This situation would not be stable if the defects were not lines. This boundary condition is, in fact, interesting in its own right, as shown in Fig. 12, where a central sink defect exhibits a weak zigzag instability. Simulations with wider domains exhibit complicated spatial structures which persist for long times.

V. CONCLUSIONS

The purpose of this work has been to study the effects of transverse boundary conditions on the traveling-wave solutions found in laser models. We have found that the observation of the traveling waves depends greatly on the system parameters. The “hard” boundary conditions imposed by reflecting walls force the presence of the source and sink defects there. The transverse size of these defects depends on the system parameters and when this size becomes comparable to the size of the transverse domain the traveling-wave solutions are no longer ob-

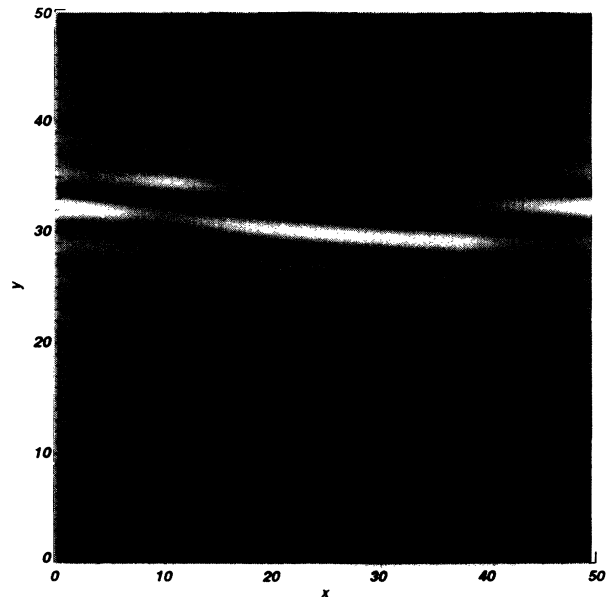


FIG. 12. Modulus of the electric field $|e|$ as a function of the two transverse coordinates (x, y) for a domain width $L \approx 50$. $a = 1$, $b = 1$, $\Delta = 4$, $\sigma = 1$, and $r = 5$. The top and bottom domain walls are reflecting and the left and right walls are periodic. The sink defect (roll pattern) in the center has developed a zigzag instability.

served in the center of the beam, only standing waves. This comparison between the defect and domain size allows the distinction to be made between small- and large-aspect-ratio laser systems. We have been able to obtain semiquantitative agreement between numerical and analytical estimates for the size of the sink defect and a scaling law has been determined.

In sufficiently large-aspect-ratio configurations we observe patterns with a large number of defects which undergo interactions. We have also observed the predicted instabilities of the source defect as a series of “blips” in one dimension and of optical vortices in two dimensions.

The links between defects and boundaries are expected to extend to other forms of boundary conditions and other domain geometries, which will be the subject of future work. In conclusion the traveling-wave laser states may be observable, but careful manipulation of bound-

ary conditions and control of defects may be necessary to obtain reasonably “pure” traveling-wave outputs in large-aspect-ratio lasers.

ACKNOWLEDGMENTS

The authors acknowledge the support of a NATO grant for this work. This work is supported in part by SERC Grants Nos. GR/F 76502 and GR/G 12665 and ESPRIT BRA 7118 (TONICS). The Arizona Center for Mathematical Sciences is sponsored by AFOSR Contract No. FQ8671-9000589 (AFOSR-90-0021). G.K.H. acknowledges the support of the SERC. G.K.H. would like to thank Rob Indik and Joceline Lega for many useful discussions.

-
- [1] L. A. Lugiato *et al.*, *J. Opt. Soc. Am. B* **7**, 1019 (1990).
 - [2] G. D'Alessandro and G.-L. Oppo, *Opt. Commun.* **88**, 130 (1992).
 - [3] P. Couillet, L. Gil, and F. Rocca, *Opt. Commun.* **73**, 403 (1989).
 - [4] P. Couillet, L. Gil, and J. Lega, *Physica D* **37**, 91 (1989).
 - [5] P. K. Jakobsen, J. V. Moloney, A. C. Newell, and R. Indik, *Phys. Rev. A* **45**, 8129 (1992).
 - [6] L. Gil, Ph.D. thesis, University of Nice, 1988.
 - [7] G.-L. Oppo, G. D'Alessandro, and W. J. Firth, *Phys. Rev. A* **44**, 4712 (1991).
 - [8] M. C. Cross and P. C. Hohenberg, *Rev. Mod. Phys.* **65**, 851 (1993).
 - [9] J. V. Moloney and A. C. Newell, *Nonlinear Optics* (Addison-Wesley, Redwood City, CA, 1991).
 - [10] M. C. Cross, *Phys. Rev. A* **38**, 3593 (1988).
 - [11] P. Manneville, *Dissipative Structure and Weak Turbulence* (Academic Press, San Diego, 1990).
 - [12] P. Couillet, T. Frisch, and F. Plaza, *Physica D* **62**, 75 (1993).
 - [13] J. Lega, P. K. Jakobsen, J. V. Moloney, and A. C. Newell, *Phys. Rev. A* **49**, 4201 (1994).
 - [14] F. H. Busse, *Rep. Prog. Phys.* **41**, 24 (1978).
 - [15] Q. Feng, J. V. Moloney, and A. C. Newell, *Phys. Rev. Lett.* **71**, 1705 (1993).
 - [16] K. D. Laakmann and W. H. Steier, *Appl. Opt.* **15**, 1334 (1976).
 - [17] W. H. Press, B. P. Flannery, S. A. Teukolsky, and W. T. Vetterling, *Numerical Recipes: The Art of Scientific Computing* (Cambridge University Press, Cambridge, 1986).

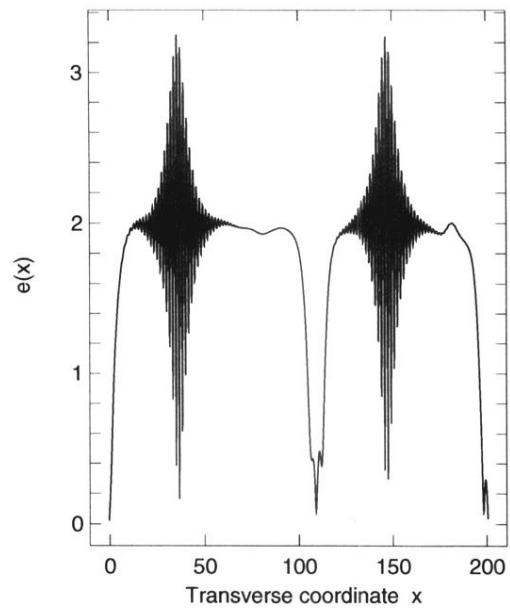


FIG. 10. Modulus of the electric field $|e|$ as a function of transverse space coordinate x for a domain width $L = 200$. $a = 1$, $b = 1$, $\Delta = 4$, $\sigma = 1$, and $r = 5$.

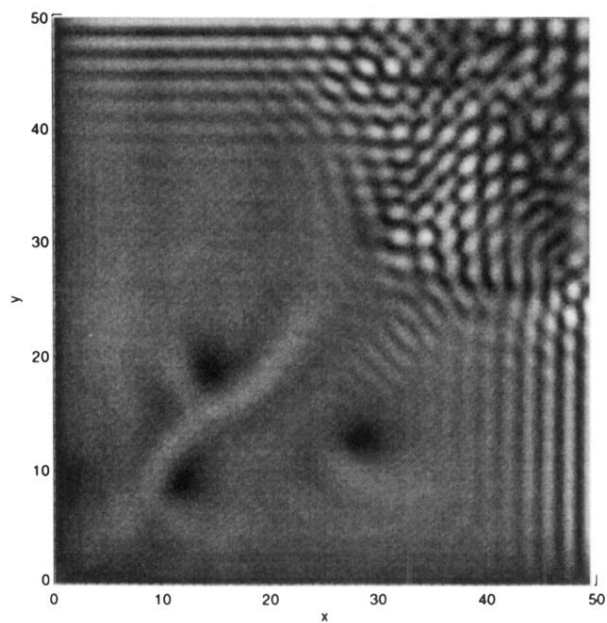


FIG. 11. Modulus of the electric field $|e|$ as a function of the two transverse coordinates (x, y) for a domain width $L \approx 50$. $a = 1$, $b = 1$, $\Delta = 4$, $\sigma = 1$, and $r = 5$. White means high intensity and black means low intensity. The three dark patches at the lower left are vortex defects, which convect with the traveling wave to the sink at the upper right.

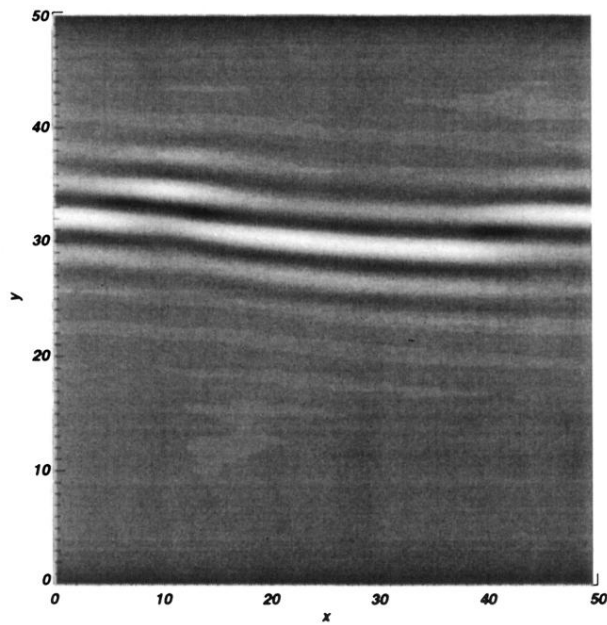


FIG. 12. Modulus of the electric field $|e|$ as a function of the two transverse coordinates (x, y) for a domain width $L \approx 50$. $a = 1$, $b = 1$, $\Delta = 4$, $\sigma = 1$, and $r = 5$. The top and bottom domain walls are reflecting and the left and right walls are periodic. The sink defect (roll pattern) in the center has developed a zigzag instability.

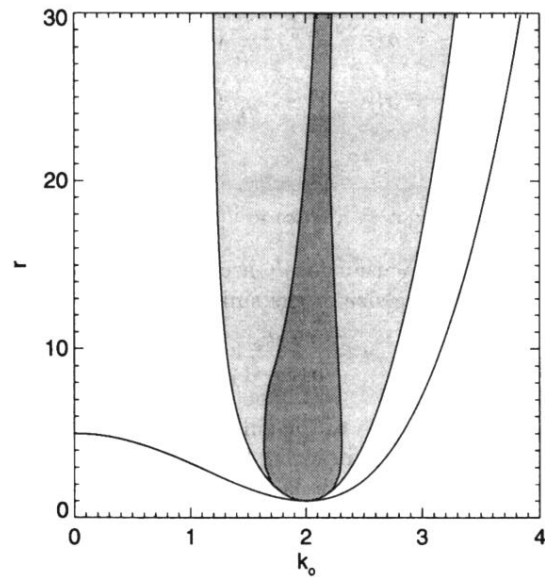


FIG. 4. Results of the stability analysis for traveling waves. Grey areas represent the Busse balloons calculated analytically from the Cross-Newell phase equation (light grey) and computed from the full stability analysis (dark grey). System parameters are $a = 1$, $b = 1$, $\Delta = 4$, and $\sigma = 1$.